Supplementary Figure Legends:

Figure S1. *Ino80* deletion ESCs.

(A) *Ino80* deletion strategy. **(B)** Karyotyping of *Ino80*-cKO ESCs. **(C-D)** *Ino80* expression at the indicated time points after 4-OHT treatment. *Ino80* mRNA expression was determined by RT-qPCR, first normalized to *Gapdh* and then normalized to day-0, and plotted as mean ± SEM from three replicates (C). *Ino80* protein expression was determined by western blot (D). Ran was used as a loading control. The experiments were repeated three times and one representative result was shown. **(E)** Genome browser track to show INO80 ChIP-seq in WT and *Ino80* deletion cells. ESCs were treated with 4-OHT for 2 days, cultured for another 2 days, and collected for ChIP-seq. **(F)** Relative live cell number of WT and *Ino80* deletion cells in naïve (Figure 1C) and primed state (Figure 1E). Cell numbers were normalized to wild type cells. The experiment was repeated three times. p-values were calculated by student *t*-test: ** <0.01.

Figure S2. INO80 ChIP-seq.

(A) HA knock-in at the endogenous *Ino80* locus. Upper: targeting strategy; Lower: Western blot using the HA and INO80 antibody. β-Actin was used as the loading control. The experiments were repeated three times and one representative result was shown. **(B-C)** Comparison of ChIP-seq using the HA and INO80 antibody in the *Ino80*-HA ESCs. Cells were cultured in serum/LIF. (B) Venn diagram to show the overlap of ChIP-seq peaks. (C) Genome browser track view of ChIP-seq signals. **(D-F)** Comparison of INO80 ChIP-seq by MNase digestion or sonication. (D) Venn diagram to show the overlap of ChIP-seq peaks. (E) Heatmap to show ChIP-seq signals in MNase-ChIP and Sonication-ChIP shared peaks(left) or MNase-specific peaks (right). Peaks were sorted by MNase-ChIP-seq signal intensity. (F) Box plots to show H3K4me3 and H3K27me3 ChIP-seq signals at MNase-specific peaks or MNase-ChIP and Sonication-ChIP shared peaks. **(G)** Distribution of INO80 ChIP-seq peaks in the genome in the naïve and primed state. **(H)** INO80 occupancy near of *Ino80* deletion-induced DEGs in the naïve and primed state. **(I)** Top gene ontology terms enriched in INO80-bound bivalent genes.

Figure S3. Establishment of bivalency during the naïve to primed transition.

(A) Metagene plots of normalized H3K27me3 ChIP-seq signals at INO80-bound H3K27me3-only TSSs. **(B-C)** Metagene plots to show normalized H3K27me3 (B) and H3K4me3 (C) ChIP-seq signals at INO80-bound bivalent TSSs in the naïve state. **(D)** Pie chart of the number of DEGs in INO80-bound bivalent genes. **(E)** Violin plots of normalized ChIP-seq signals of H3K4me3 (upper) and H3K27me3 (lower) on the primed bivalent promoters during the naïve to primed transition (based on public data GSE117896). **(F)** Genome browser track of H3K4me3 and H3K27me3 occupancy near T during the naïve to primed transition (based on public data GSE117896). **(G)** Genome browser track to show INO80, H3K4me3 and H3K27me3 occupancy near T during the naïve to primed transition (from this study). **(H)** Relative live cell number of WT and *Ino80* deletion cells in naïve to primed transition as Figure 4F. Cell numbers were normalized to wild type cells. The experiment was repeated three times. p-values were calculated by student *t*-test: *** <0.001.

Figure S4. The requirement for INO80 chromatin remodeling activity.

(A) Strategy to generate the INO80 ATPase-dead mutant cells and Western blot to show the expression of the Dox-inducible WT and ATPase-dead INO80 expression. *Ino80* conditional deletion ESCs were transfected with piggyBac vectors expressing Dox-inducible WT or ATPase-dead *Ino80* (KA or EQ mutant), puromycin selected and cultured in 2iL. *Ino80* deletion was induced by 4-OHT treatment and exogenous *Ino80* expression was induced by Dox treatment. Cells were harvested and INO80 expression was detected

by western blot using the INO80 antibody. β-actin was used for loading control. The experiment was repeated three times and one representative result was shown. **(B)** Relative live cell number of WT and *Ino80* deletion cells expressing WT or INO80 ATPase-dead mutant as Figure 5A. Cell numbers were normalized to wild type cells. The experiment was repeated three times. p-values were calculated by student *t*-test: *** <0.001. **(C-E)** *Ino80*-KA/ED knock-in ESCs. ATPase-dead mutations were introduced into the endogenous *Ino80* in E14Tg2a cells by CRISPR-mediated genome editing. Protein expression of the WT and mutant INO80 was determined by western blot in WT and *Ino80* homozygous knock-in cells cultured in 2iL (C). WT and *Ino80*-KA/ED knock-in ESCs were cultured in FA and cell morphology was examined by imaging (D). The expression of representative bivalent genes was determined by RT-qPCR, first normalized to *Gapdh* and then normalized to wild-type cells, and plotted as mean ± SEM (E) from three independent experiments. p-values were calculated by student *t*-test: * <0.05, ** <0.01, *** <0.001. **(F-G)** Expression of the naïve-specific genes in WT and *Ino80*-KA/ED knock-in ESCs (F) or WT and *Ino80*-deletion ESCs (G) during the naïve to primed transition. Gene expression was determined by RT-qPCR, first normalized to *Gapdh* and then normalized to wild-type cells in 2i, and plotted as mean ± SEM from three independent experiments. **(H)** Bioanalyzer gel image to show titrated MNase digestion of WT and *Ino80* deletion cells cultured in the naïve (2iL) and primed (FAX) state. **(I)** Metagene plots of nucleosome signals at TSSs of *Ino80*-deletion induced DEGs and non-DEGs in the naïve and primed state. DEGs were separated into up- and down-regulated genes.

Figure S5. INO80 in H2A.Z occupancy.

(A) Spearman correlation of the genomic occupancy of H2A.Z and chromatin remodelers. ChIP-seq data for INO80 and H2A.Z was from this study, and ChIP-seq data for the other chromatin remodelers was from the public dataset GSE64825. **(B)** H2A.Z ChIP-seq peak distribution in the genome in the naïve and primed state. **(C)** H2A.Z ChIP-seq signals in the naïve and primed state. **(D-E)** Western blots of H2A.Z in WT and Ino80 deletion cells. Histone H3 was used as a loading control (D). For quantitation, H2A.Z expression was normalized by H3 and then to wild-type cells in the naïve state by ImageJ (E). The experiment was repeated three times and one representative result was shown. **(F)** Metagene plot to show normalized H2A.Z ChIP-seq signals at active promoters and enhancer regions in wild-type and *Ino80* deletion cells in the primed state. **(G-H)** Metagene (G) and box plots (H) of normalized H2A.Z ChIP-seq signals at the INO80-bound bivalent promoters in the naïve state in WT and *Ino80* deletion cells. p-value was calculated by Wilcoxon assigned rank test. **(I-J)** Ino80 deletion in MEFs. MEFs were treated with DMSO or 4-OHT for 2 days. Cells were imaged (I) and collected for H2A.Z ChIP-seq at day-4. Normalized H2A.Z ChIP-seq signal at INO80-bound TSSs was shown in the box plot (J).

Figure S6. H2A.Z and bivalency.

(A) Overlap between INO80-bound bivalent TSSs and H2A.Z peaks in the primed state. **(B)** Violin plot of normalized H2A.Z ChIP-seq signals at promoters of INO80-bound active, INO80-bound bivalent and non-INO80-bound gene promoters in the primed state. **(C)** Strategy of *H2az1*/*H2az2* inducible deletion in Rosa26::Cre-ERT2 ESCs. **(D)** Expression of H2A.Z in WT and *H2az1*/*H2az2* deletion ESCs. *H2az1*-cKO/*H2az2*-KO ESCs were treated with DMSO or 4-OHT. H2A.Z mRNA expression was determined by RT-qPCR, first normalized by *Gapdh* and then normalized to wild-type cells, and plotted as mean ± SEM from three replicates. **(E)** H2A.Z protein expression was determined by western blot. β-actin and histone H3 were used as loading controls. **(F)** MA analysis to show changes in H3K27me3 occupancy at INO80-bound bivalent TSSs in WT and *H2az1*-cKO/*H2az2*-KO ESCs.

Figure S7. INO80 and H2A.Z regulate PRC2.

(A-B) Western blots to show protein levels of H2A.Z, PRC2 components SUZ12 and EZH2 in WT and *Ino80* deletion (A) and H2A.Z deletion cells (B) in the primed state. β-actin was used as loading control. The experiment was repeated three times and one representative result was shown. **(C)** Venn diagram to show the overlap of H2AZ peaks in WT, *Eed*-KO and *Ezh2*-KO ESCs. Cells were cultured in FAX and collected for H2A.Z ChIP-seq. **(D)** Box plot of normalized H2A.Z ChIP-seq signals of all H2A.Z peaks in (C). **(E)** Heatmap of normalized H2A.Z ChIP-seq signals at the primed bivalent promoters in WT, *Eed*-KO and *Ezh2*-KO ESCs. **(F-G)** ChIP-qPCRs to show H2A.Z (F) and SUZ12 (G) at representative bivalent gene promoters in *Ino80* deletion cells expressing WT and ATPase-dead mutant INO80 as in Figure 5B. Fold enrichment was plotted as mean ± SEM and p-values were calculated by student *t*-test: * <0.05, ** <0.01, *** <0.001. The experiment was repeated twice and shown as exp1 and exp2.

Supplemental Tables

Table S1: Antibodies used in this study.

Table S2: Primers for RT-qPCR, ChIP-qPCR and oligos for genome targeting.

Table S3: Software and algorithms used for data analysis.

Figure S1

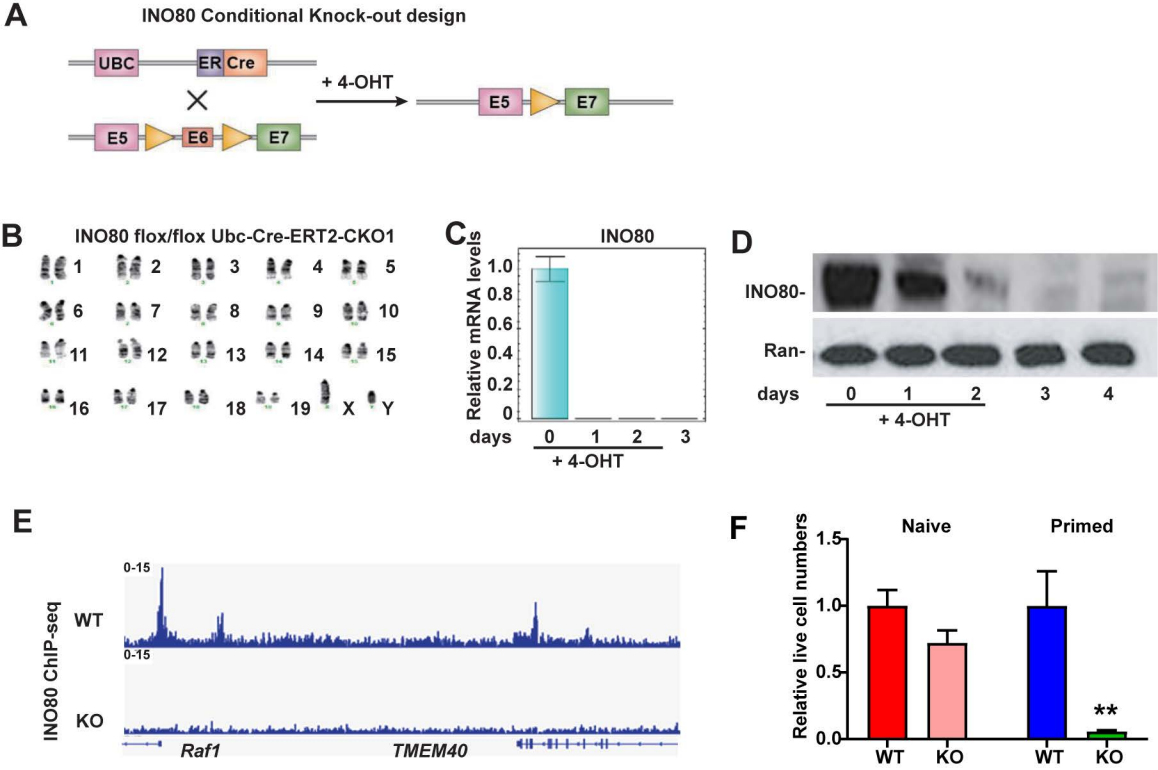
A
INO80 Conditional Knock-out design
UBC
ER Cre
+ 4-OHT
E5
E6
E7
B
INO80 flox/flox Ubc-Cre-ERT2-CKO1
C
INO80
Relative mRNA levels
days
+ 4-OHT
D
INO80-
Ran-
days
+ 4-OHT
E
INO80 ChIP-seq
WT
KO
Raf1
TMEM40
F
Naive
Primed
Relative live cell numbers
WT
KO

Figure S2

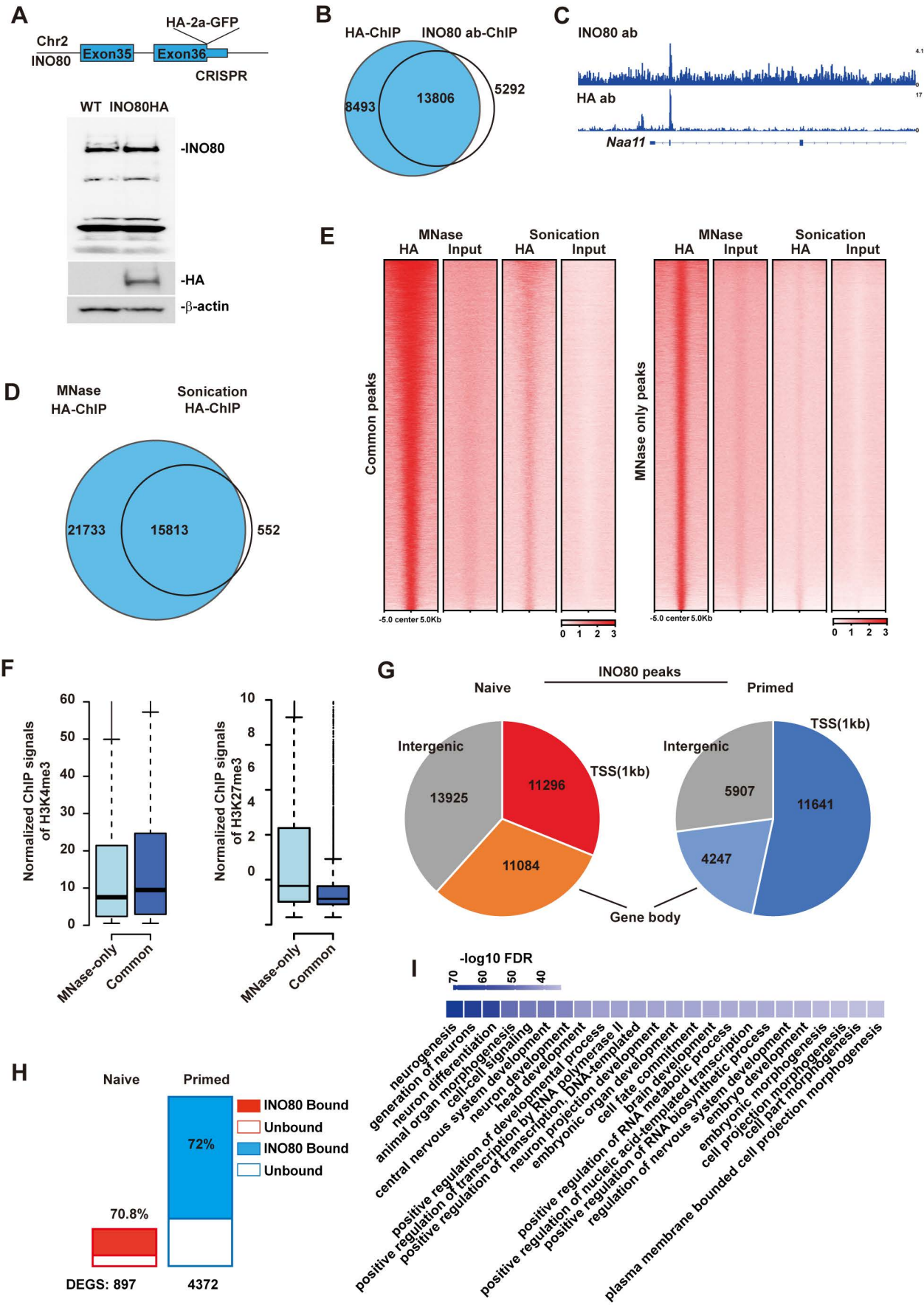
A
HA-2a-GFP
Chr2
INO80
Exon35
Exon36
CRISPR
WT INO80HA
-INO80
-HA
-β-actin
B
HA-ChIP
INO80 ab-ChIP
8493
13806
5292
C
INO80 ab
HA ab
Naa11
D
MNase
HA-ChIP
Sonication
HA-ChIP
21733
15813
552
E
MNase
Sonication
HA
Input
Common peaks
MNase only peaks
-5.0 center 5.0Kb
0 1 2 3
F
Normalized ChIP signals of H3K4me3
Normalized ChIP signals of H3K27me3
MNase-only
Common
G
INO80 peaks
Naive
Primed
Intergenic
TSS(1kb)
Gene body
13925
11296
11084
5907
11641
4247
H
Naive
Primed
INO80 Bound
Unbound
72%
70.8%
DEGS: 897
4372
I
-log10 FDR
neurogenesis
generation of neurons
neuron differentiation
animal organ morphogenesis
cell-cell signaling
central nervous system development
neuron development
head development
positive regulation of developmental process
positive regulation of transcription by RNA polymerase II
positive regulation of transcription, DNA-templated
neuron projection development
embryonic organ development
cell fate commitment
brain development
positive regulation of RNA metabolic process
positive regulation of nucleic acid-templated transcription
positive regulation of RNA biosynthetic process
regulation of nervous system development
embryonic development
embryo development
embryonic morphogenesis
cell projection morphogenesis
plasma membrane bounded cell projection morphogenesis
cell part morphogenesis

Figure S3

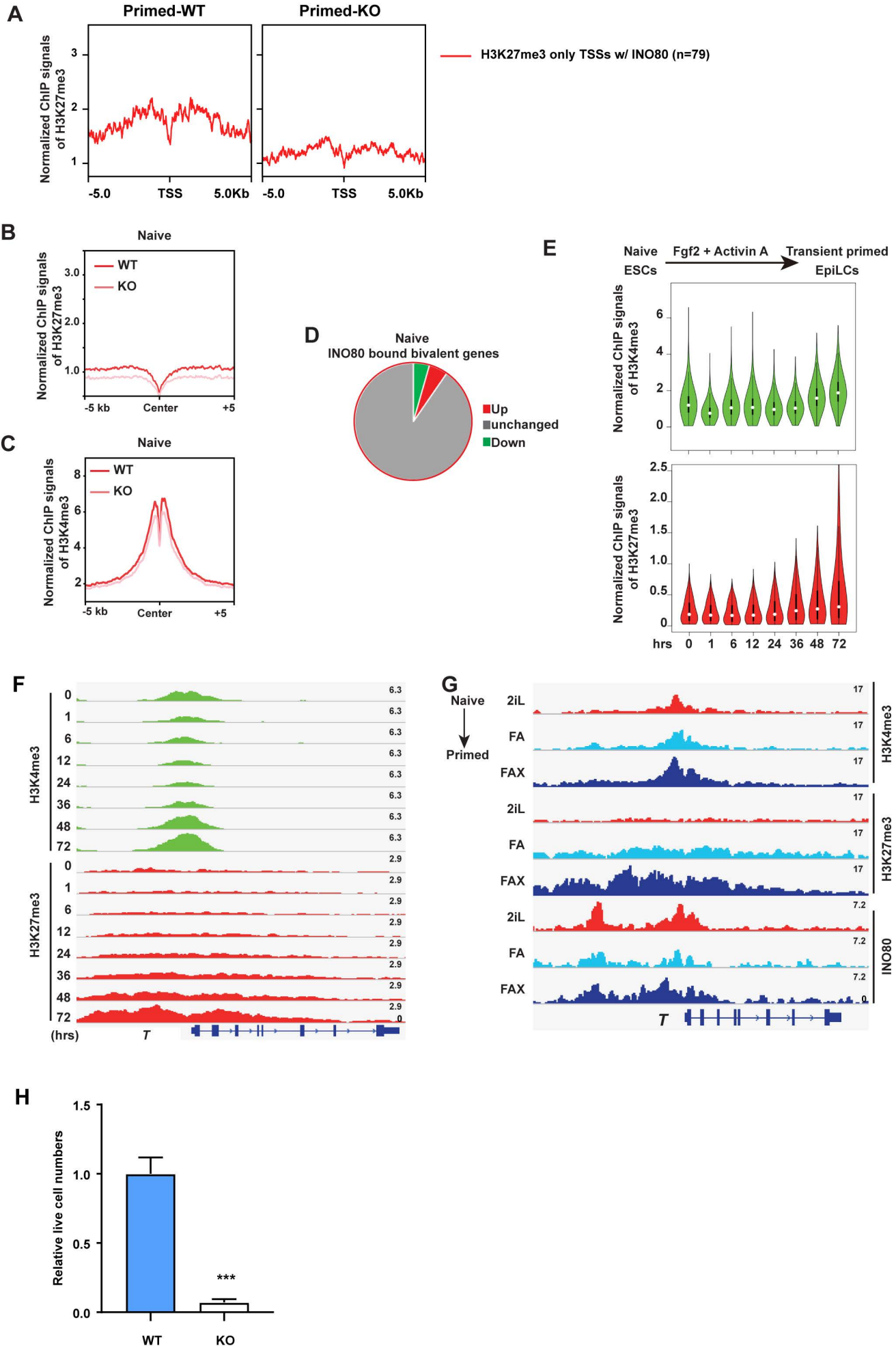
A
Primed-WT
Primed-KO
Normalized ChIP signals of H3K27me3
H3K27me3 only TSSs w/ INO80 (n=79)
-5.0
TSS
5.0Kb
B
Naive
WT
KO
Normalized ChIP signals of H3K27me3
-5 kb
Center
+5
C
Naive
WT
KO
Normalized ChIP signals of H3K4me3
D
Naive
INO80 bound bivalent genes
Up
unchanged
Down
E
Naive ESCs
Fgf2 + Activin A
Transient primed EpiLCs
Normalized ChIP signals of H3K4me3
Normalized ChIP signals of H3K27me3
hrs 0 1 6 12 24 36 48 72
F
H3K4me3
H3K27me3
(hrs)
G
Naive
Primed
2iL
FA
FAX
H3K4me3
H3K27me3
INO80
H
Relative live cell numbers
***
WT
KO

Figure S4

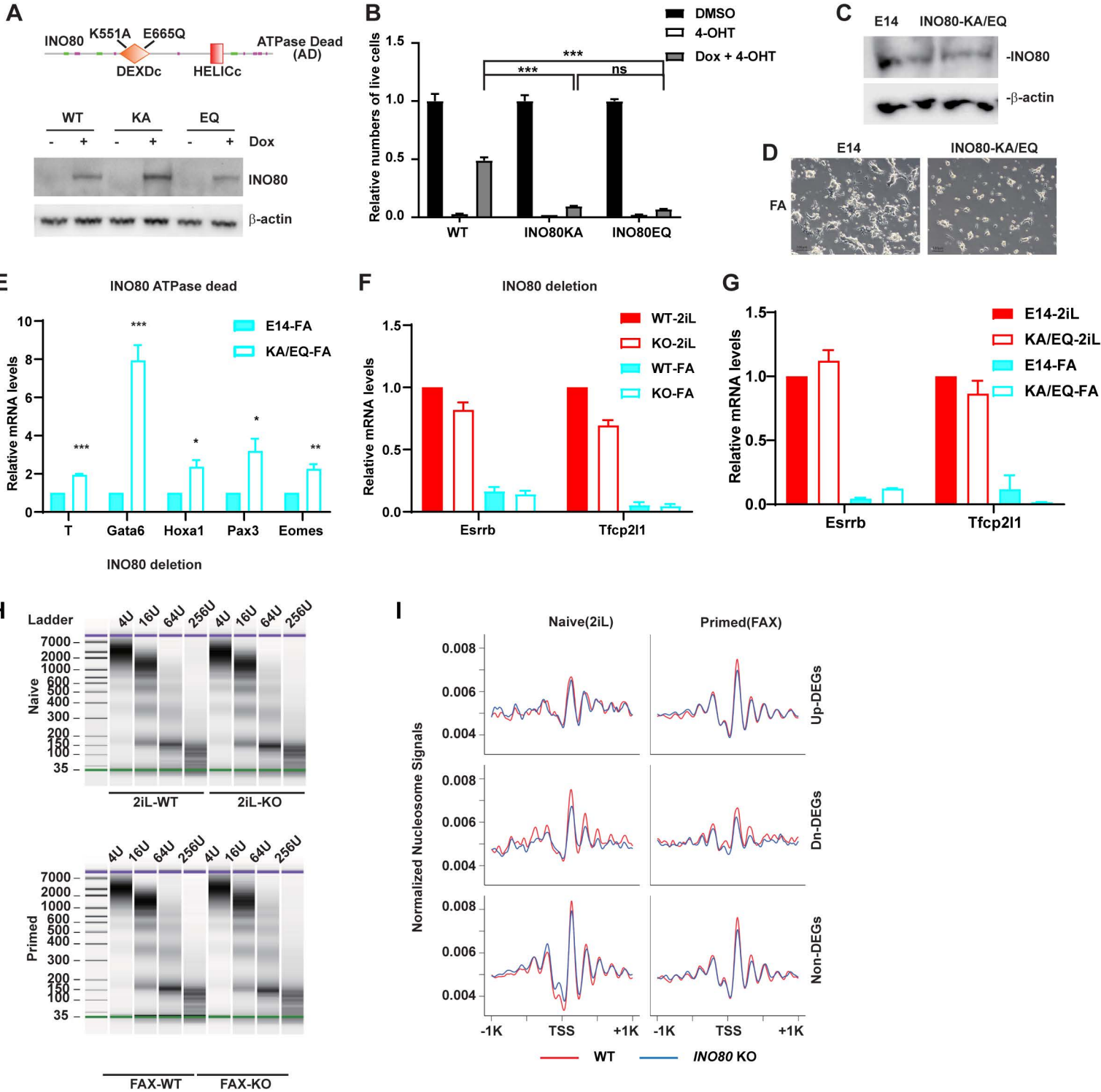
A
INO80
K551A
E665Q
ATPase Dead (AD)
DEXDc
HELICc
WT
KA
EQ
Dox
INO80
β-actin
B
DMSO
4-OHT
Dox + 4-OHT
Relative numbers of live cells
***
***
ns
WT
INO80KA
INO80EQ
C
E14
INO80-KA/EQ
-INO80
-β-actin
D
E14
INO80-KA/EQ
FA
E
INO80 ATPase dead
E14-FA
KA/EQ-FA
Relative mRNA levels
T
Gata6
Hoxa1
Pax3
Eomes
INO80 deletion
F
INO80 deletion
WT-2iL
KO-2iL
WT-FA
KO-FA
Relative mRNA levels
Esrrb
Tfcp2l1
G
E14-2iL
KA/EQ-2iL
E14-FA
KA/EQ-FA
Relative mRNA levels
Esrrb
Tfcp2l1
H
Ladder
4U
16U
64U
256U
Naive
2iL-WT
2iL-KO
Primed
FAX-WT
FAX-KO
I
Naive(2iL)
Primed(FAX)
Normalized Nucleosome Signals
Up-DEGs
Dn-DEGs
Non-DEGs
-1K
TSS
+1K
WT
INO80 KO

Figure S5

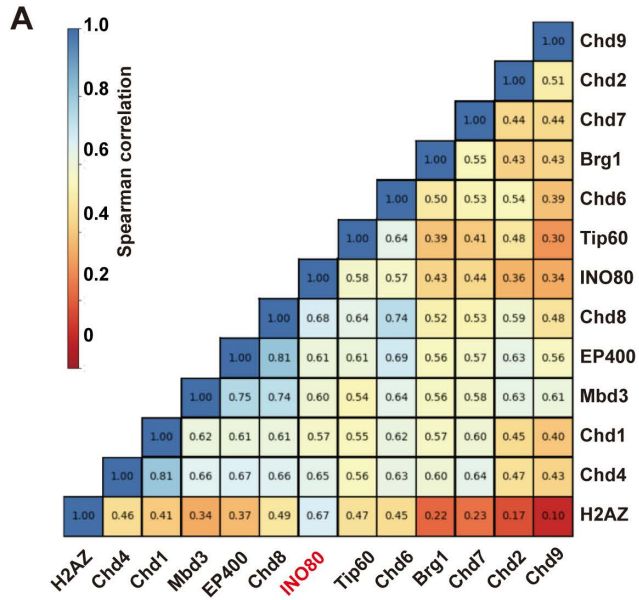
A
Spearman correlation
1.0
0.8
0.6
0.4
0.2
0
Chd9
Chd2
Chd7
Brg1
Chd6
Tip60
INO80
Chd8
EP400
Mbd3
Chd1
Chd4
H2AZ
H2AZ Chd4 Chd1 Mbd3 EP400 Chd8 INO80 Tip60 Chd6 Brg1 Chd7 Chd2 Chd9

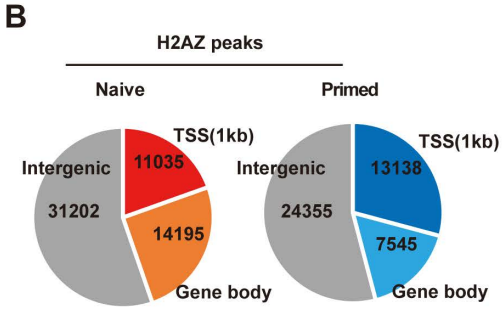
B
H2AZ peaks
Naive
Primed
Intergenic
31202
TSS(1kb)
11035
14195
Gene body
Intergenic
24355
TSS(1kb)
13138
7545
Gene body

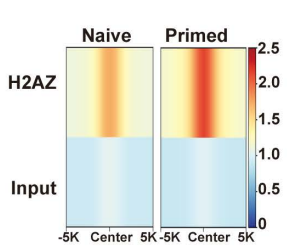
C
Naive
Primed
H2AZ
Input
2.5
2.0
1.5
1.0
0.5
0
-5K Center 5K
-5K Center 5K

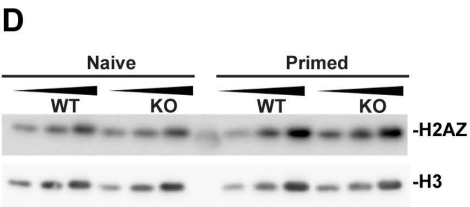
D
Naive
Primed
WT
KO
WT
KO
-H2AZ
-H3

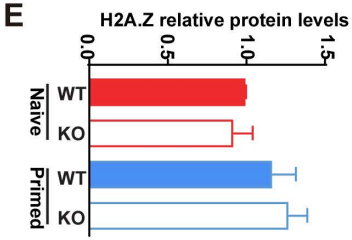
E
H2A.Z relative protein levels
0.0
0.5
1.0
1.5
Naive
WT
KO
Primed
WT
KO

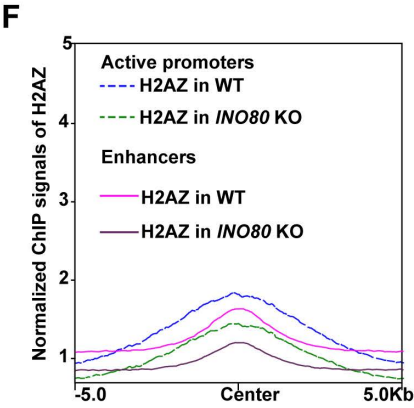
F
Active promoters
H2AZ in WT
H2AZ in INO80 KO
Enhancers
H2AZ in WT
H2AZ in INO80 KO
Normalized ChIP signals of H2AZ
5
4
3
2
1
-5.0
Center
5.0Kb

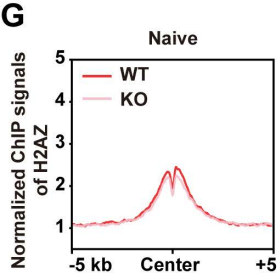
G
Naive
WT
KO
Normalized ChIP signals of H2AZ
5
4
3
2
1
-5 kb
Center
+5

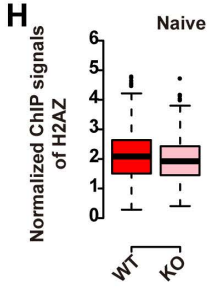
H
Naive
Normalized ChIP signals of H2AZ
6
5
4
3
2
1
0
WT
KO

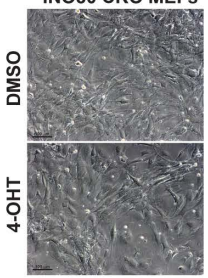
I
INO80 CKO MEFs
DMSO
4-OHT

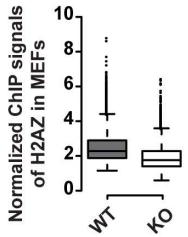
J
Normalized ChIP signals of H2AZ in MEFs
10
8
6
4
2
0
WT
KO

Figure S6

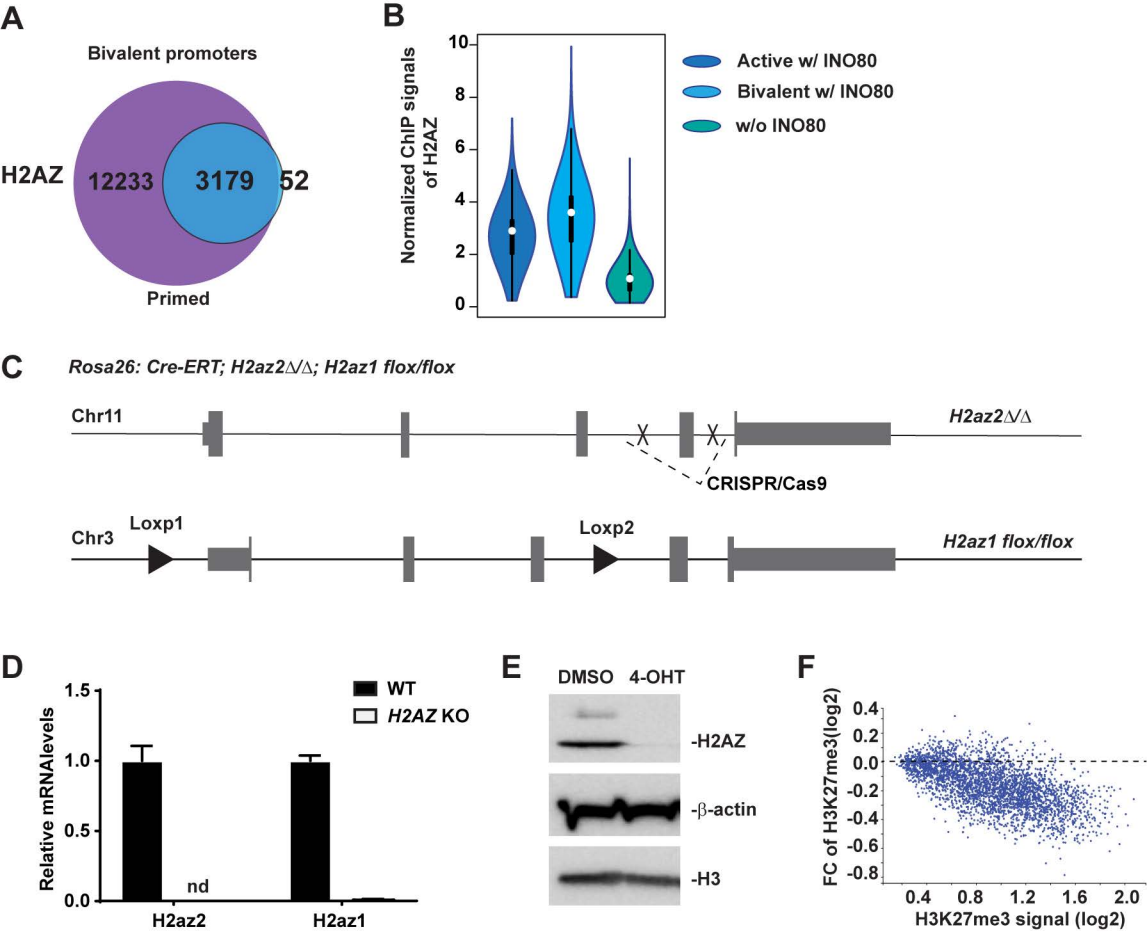
A
Bivalent promoters
H2AZ
12233
3179
52
Primed
B
Normalized ChIP signals of H2AZ
10
8
6
4
2
0
Active w/ INO80
Bivalent w/ INO80
w/o INO80
C
Rosa26: Cre-ERT; H2az2Δ/Δ; H2az1 flox/flox
Chr11
H2az2Δ/Δ
CRISPR/Cas9
Chr3
Loxp1
Loxp2
H2az1 flox/flox
D
Relative mRNAlevels
1.5
1.0
0.5
0.0
WT
H2AZ KO
nd
H2az2
H2az1
E
DMSO
4-OHT
-H2AZ
-β-actin
-H3
F
FC of H3K27me3(log2)
0.4
0.2
0.0
-0.2
-0.4
-0.6
-0.8
0.4
0.8
1.2
1.6
2.0
H3K27me3 signal (log2)

Figure S7

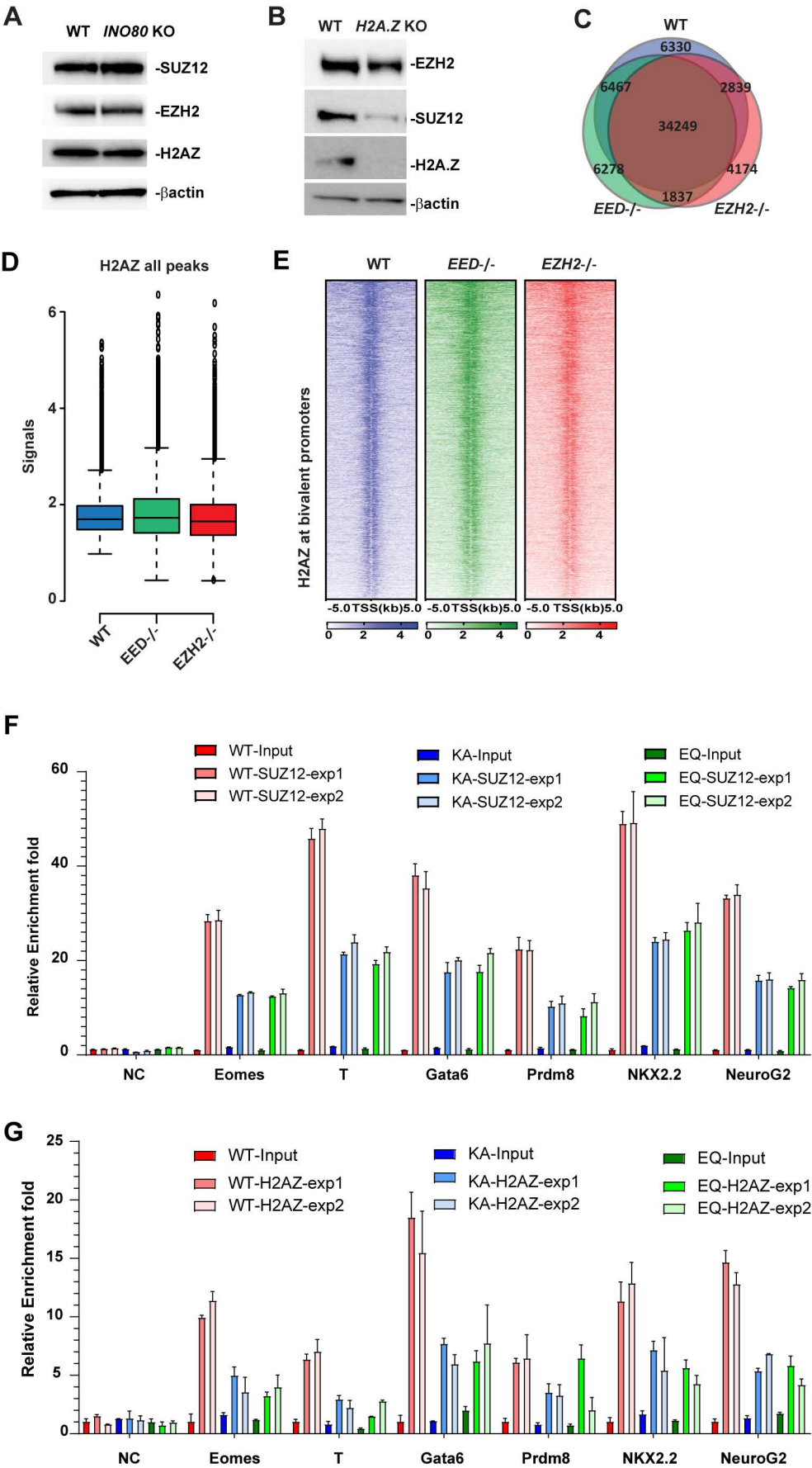
A
WT
INO80 KO
-SUZ12
-EZH2
-H2AZ
-βactin
B
WT
H2A.Z KO
-EZH2
-SUZ12
-H2A.Z
-βactin
C
WT
6330
6467
2839
34249
6278
4174
1837
EED-/-
EZH2-/-
D
H2AZ all peaks
Signals
6
4
2
0
WT
EED-/-
EZH2-/-
E
WT
EED-/-
EZH2-/-
H2AZ at bivalent promoters
-5.0 TSS(kb) 5.0
0 2 4
F
WT-Input
WT-SUZ12-exp1
WT-SUZ12-exp2
KA-Input
KA-SUZ12-exp1
KA-SUZ12-exp2
EQ-Input
EQ-SUZ12-exp1
EQ-SUZ12-exp2
Relative Enrichment fold
60
40
20
0
NC
Eomes
T
Gata6
Prdm8
NKX2.2
NeuroG2
G
WT-Input
WT-H2AZ-exp1
WT-H2AZ-exp2
KA-Input
KA-H2AZ-exp1
KA-H2AZ-exp2
EQ-Input
EQ-H2AZ-exp1
EQ-H2AZ-exp2
Relative Enrichment fold
25
20
15
10
5
0
NC
Eomes
T
Gata6
Prdm8
NKX2.2
NeuroG2

Table S1: Antibodies used in this study.

	WB	ChIP-seq	Vendor	Cat#
H3	√		Abcam	ab1791
Ran	√		BD	610341
b-actin	√		Sigma	A5316
INO80	√	√	ProteinTech	18810-1-AP
HA	√	√	Cell Signaling	#3724
H2AZ	√	√	Active motif	39943
EZH2		√	Cell Signaling	#5246
SUZ12		√	Cell Signaling	#3737
H3K4me3		√	Active motif	39159
H3K27me3		√	Active motif	39155
H3K27ac		√	Abcam	ab4729

Table S2: Primers for RT-qPCR, ChIP-qPCR and oligos for genome targeting.

qPCR primers	Forward	Reward
Nanog	AAGCAGAAGATGCGGACTGT	ATCTGCTGGAGGCTGAGGTA
Esrrb	CGATTCATGAAATGCCTCAA	CCTCCTCGAACTCGGTCA
Fgf5	GAAAAGACAGGCCGAGAGTG	GAAGTGGGTGGAGACGTGTT
Ino80	TTCACAACATGCTTCGATTACAC	AAGCAAGTGGCGCTGTTG
Gapdh	GTCGTGGAGTCTACTGGTGTC	GAGCCCTTCCACAATGCCAAA
Nestin	GACCCTGCTTCTCCTGCTC	CTGCAGGCCACTGAAAAGTT
Brachy(T)	CAGCCCACCTACTGGCTCTA	GAGCCTGGGGTGATGGTA
Eomes	ACCCGACCTTCCCTGCTATG	GTGGGCTCATTCTGGATGTC
Gata2	CTACCACAAGATGAATGGACAGA	TGTCGTCTGACAATTTGCACAAC
Gata4	CATGGCCCCACAATTGAC	GGAAGACACCCCAATCTCG
Gata6	TGGCACAGGACAGTCCAAG	GGTCTCTACAGCAAGATGAATGG
H2az1	GGCCGTATTCATCGACACCT	GACGAGGGGTGATACGCTTT
H2az2	TACAGTGCCGCAATTCTGGA	CTCTTCATCACCGCGGATTG
Hoxa1	CCTGGAGTGATGTGGTCCAG	AGCAACCACTGTAGTCCAGC
Hoxa5	TCCACCCAACTCCCCCATTA	GGGACATGTACTCGGTTCCC
Pax3	AACCCACTACCCAGACATTTA	GGCCGGTTGCTAAACCAGAC
Tfcp2l1	CAGCCCGAACACTACAACCAG	CAGCCGGATTTCATACGACTG
Foxa2	CGAGCTAAAGGGAGCACCT	TAATGGTGCTCGGGCTTC
Sox9	ATCTGCACAACGCGGAGCTCA	CTCTTCTCGCTCTCGTTCAGCAG
TBX4	TCCCCAGCTACAAGGTAAAAGT	ACCATCCATTTGTTGTCACAGAA

sgRNA	
H2az2-sg1	ACACGTACACAGGAAAAACC
H2az2-sg2	TGTAGCACATTTAACACGTA
H2az1-loxp1sg	AGAGGCGCCGGTTGTCAGCG
H2az1-loxp2sg	TGCAATTGCGTGCCCCTTCG
INO80-HAStopsg	CCTCTGGAGGACGGTAACCA
INO80KAsg	CTTGCTGATGAAATGGGTCT
INO80EQsg	CATGGTACTGGATGAAGCTC

ChIP primer	Forward	Reward
negative	ACCTAGTCCTAGCCAAGCCA	TGTGGCATCTGGCTCATCTG
Prdm8	CACGAAATCGTTCACGCCTC	TATCGCATGCATCAGGGGTC
T	TACTTCAAAGGGTGTCCCGC	AGGCGCGACAAGAGTAAGTC
Gata6	GGGCGCTTCGTGAGTAGTTA	ATTAAGCGCCCGACATTCCA
Hoxa1	GTCGATGGTACTCAACGCCA	CCTACTACGACAGCTCAGCG
Nkx2.2	TCGTAGGTCTGCGCTTTGGAG	GACGAGTCACCGGACAATGACAA

Table S3. Software and Algorithms

Bowtie (v1.1.2)	(Langmead et al., 2009)	http://bowtie-bio.sourceforge.net/bowtie2/index.shtml
Cutdapt (v1.9)	(Martin, 2011)	https://cutadapt.readthedocs.io/en/v1.9/installation.html
Samtools (v1.3.1)	(Li et al., 2009)	http://samtools.sourceforge.net/
Bedtools (v2.21.0)	(Quinlan, 2014)	https://bedtools.readthedocs.io/en/latest/
Deeptools (v3.3.0)	(Ramirez et al., 2016)	https://deeptools.readthedocs.io/en/develop/
STAR (v2.5.2b)	(Dobin et al., 2013)	https://github.com/alexdobin/STAR
DESeq2 1.16.1	(Love et al., 2014)	https://bioconductor.org/packages/release/bioc/html/DESeq2.html
normalize.loess R affy package	(Cleveland, 1992; Gautier et al., 2004)	https://www.rdocumentation.org/packages/affy/versions/1.50.0/topics/normalize.loess
bedGraphToBigWig	(Kent et al., 2010)	https://www.encodeproject.org/software/bedgraphtobigwig/
R 3.3.0	R Development Core Team, 2016	https://www.r-project.org/
BoxplotR	(Spitzer et al., 2014)	https://github.com/VizWizard/BoxPlotR.shiny/blob/master/README.md

Reference for software and algorithms

Cleveland, W.S., Grosse, E., Shyu, W.M. (1992). Statistical Models in S. In Local regression models, J.M. Chambers, Hastie, T.J., ed. (Wadsworth & Brooks/Cole).

Dobin, A., Davis, C.A., Schlesinger, F., Drenkow, J., Zaleski, C., Jha, S., Batut, P., Chaisson, M., and Gingeras, T.R. (2013). STAR: ultrafast universal RNA-seq aligner. Bioinformatics *29*, 15-21.

Gautier, L., Cope, L., Bolstad, B.M., and Irizarry, R.A. (2004). affy--analysis of Affymetrix GeneChip data at the probe level. Bioinformatics *20*, 307-315.

Kent, W.J., Zweig, A.S., Barber, G., Hinrichs, A.S., and Karolchik, D. (2010). BigWig and BigBed: enabling browsing of large distributed datasets. Bioinformatics *26*, 2204-2207.

Langmead, B., Trapnell, C., Pop, M., and Salzberg, S.L. (2009). Ultrafast and memory-efficient alignment of short DNA sequences to the human genome. Genome Biology *10*, R25.

Li, H., Handsaker, B., Wysoker, A., Fennell, T., Ruan, J., Homer, N., Marth, G., Abecasis, G., Durbin, R., and Genome Project Data Processing, S. (2009). The Sequence Alignment/Map format and SAMtools. Bioinformatics *25*, 2078-2079.

Love, M.I., Huber, W., and Anders, S. (2014). Moderated estimation of fold change and dispersion for RNA-seq data with DESeq2. Genome Biology *15*.

Martin, M. (2011). Cutadapt removes adapter sequences from high-throughput sequencing reads. 2011 *17*, 3 %J EMBnet.journal.

Quinlan, A.R. (2014). BEDTools: The Swiss-Army Tool for Genome Feature Analysis. Curr Protoc Bioinformatics *47*, 11 12 11-34.

Ramirez, F., Ryan, D.P., Gruning, B., Bhardwaj, V., Kilpert, F., Richter, A.S., Heyne, S., Dundar, F., and Manke, T. (2016). deepTools2: a next generation web server for deep-sequencing data analysis. Nucleic Acids Res *44*, W160-165.

Spitzer, M., Wildenhain, J., Rappsilber, J., and Tyers, M. (2014). BoxPlotR: a web tool for generation of box plots. Nat Methods *11*, 121-122.